Geophysical Research Letters

RESEARCH LETTER
10.1029/2018GL079044

Simultaneous Multispacecraft Probing of Electron Phase Space Holes

Y. Tong[1,2], I. Vasko[1,3], F. S. Mozer[1], S. D. Bale[1,2], I. Roth[1], A.V. Artemyev[3,4], R. Ergun[5], B. Giles[6], P.-A. Lindqvist[7], C.T. Russell[4], R. Strangeway[4], and R. B. Torbert[8]

[1]Space Sciences Laboratory, University of California, Berkeley, CA, USA, [2]Department of Physics, University of California, Berkeley, CA, USA, [3]Space Research Institute of Russian Academy of Sciences, Moscow, Russia, [4]Institute of Geophysics and Planetary Sciences, University of California, Los Angeles, CA, USA, [5]Laboratory for Atmospheric and Space Physics, University of Colorado Boulder, Boulder, CO, USA, [6]NASA Goddard Space Flight Center, Greenbelt, MD, USA, [7]Department of Space and Plasma Physics, KTH Royal Institute of Technology, Stockholm, Sweden, [8]Department of Physics, University of New Hampshire, Durham, NH, USA

Abstract We present a series of electron holes observed simultaneously on four Magnetospheric Multiscale spacecraft in the plasma sheet boundary layer. The multispacecraft probing shows that the electron holes propagated quasi-parallel to the local magnetic field with velocities of a few thousand kilometers per second with parallel spatial scales of a few kilometers (a few Debye lengths). The simultaneous multispacecraft probing allows analyzing the 3-D configuration of the electron holes. We estimate the electric field gradients and charge densities associated with the electrons holes. The electric fields are fit to simple 3-D electron hole models to estimate their perpendicular scales and demonstrate that the electron holes were generally not axially symmetric with respect to the local magnetic field. We emphasize that most of the electron holes had a complicated structure not reproduced by the simple models widely used in single-spacecraft studies.

Plain Language Summary We present the first measurement of electron holes (electrostatic solitary waves) by four Magnetospheric Multiscale spacecraft simultaneously. Such observation has allowed us to directly measure the charge density and to address the 3-D structure of these electron holes both for the first time. The analysis of 3-D configuration of the electron holes can be valuable for analysis of electron holes observed in space plasmas.

Key Points:
- Simultaneous observations of electron phase space holes at four MMS spacecraft are presented
- The charge density within the electron holes is computed using the electric field measurements at four spacecraft
- The three-dimensional configuration of the electron holes is analyzed, and the perpendicular scales are estimated

Supporting Information:
- Supporting Information S1

Correspondence to:
Y. Tong,
ygtong@berkeley.edu

Citation:
Tong, Y., Vasko, I., Mozer, F. S., Bale, S. D., Roth, I., Artemyev, A. V., et al. (2018). Simultaneous multispacecraft probing of electron phase space holes. *Geophysical Research Letters*, *45*, 11,513–11,519. https://doi.org/10.1029/2018GL079044

Received 1 JUN 2018
Accepted 13 OCT 2018
Accepted article online 19 OCT 2018
Published online 4 NOV 2018

1. Introduction

Electron phase space holes (EHs) are electrostatic solitary waves (ESWs) with a bipolar parallel electric field, whose existence is due to phase space density deficit of electrons trapped by the bipolar electric field (e.g., review by Schamel, 1986). Simulations suggest that EHs are formed in a nonlinear stage of various streaming instabilities and can be stable for thousands of plasma periods (e.g., Omura et al., 1996). They were originally observed in the plasma sheet boundary layer (Matsumoto et al., 1994) and later in reconnecting current sheets (Cattell et al., 2005; Graham et al., 2016), auroral region (Ergun et al., 1998; Mozer et al., 1997), inner magnetosphere (Malaspina et al., 2015; Mozer et al., 2015), flow braking region (Ergun et al., 2015), and many other regions of the near-Earth space (e.g., Pickett et al., 2004, 2008). Similar EHs were reproduced in laboratory plasma experiments (e.g., Fox et al., 2008). Numerical simulations and theoretical analyses showed that EHs can efficiently scatter electrons, thereby contributing to anomalous dissipation processes (e.g., Drake et al., 2003; Vasko et al., 2018).

EHs in the auroral region (Ergun et al., 1998; Franz et al., 2000), inner magnetosphere (Malaspina et al., 2018; Vasko et al., 2017), and flow braking region (Ergun et al., 2015) exhibit noticeable perpendicular electric fields with essentially unipolar profiles. The perpendicular electric fields indicate that EHs are intrinsically three-dimensional structures localized in directions perpendicular to the local magnetic field. Single-spacecraft measurements showed that the perpendicular and parallel spatial scales of EHs statistically satisfy the gyrokinetic scaling relation (Franz et al., 2000): $d_\perp/d_\parallel \sim (1+\omega_p^2/\omega_c^2)^{1/2}$, where ω_p and ω_c are electron plasma and cyclotron frequencies. The laboratory experiments reported EHs with similar perpendicular

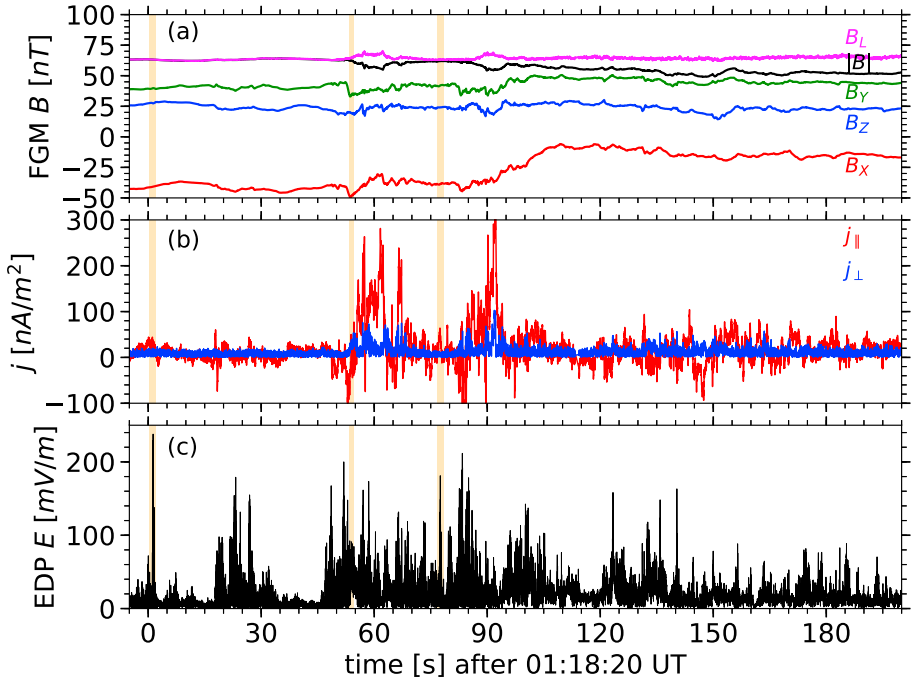

Figure 1. MMS observations on 27 September 2016 around 01:19:00 UT: (a) direct current-coupled magnetic field measured aboard MMS#4 in the geocentric solar magnetospheric coordinate system; B_L is an estimate of the magnetic field in the lobes; (b) current density parallel to the magnetic field and magnitude of the current density perpendicular to the magnetic field; (c) magnitude of alternating current-coupled electric field measured by MMS#4. Highlighted intervals indicate observations of electrostatic solitary waves. Two of the intervals are expanded in Figure 2 for further analysis. MMS = Magnetospheric Multiscale. FGM = Fluxgate Magnetometer; EDP=Electric Field Double Probes.

and parallel spatial scales in the regime $\omega_p \gg \omega_c$, indicating that the gyrokinetic scaling relation may not be universal (Fox et al., 2008).

Most of EH studies have been limited to single-spacecraft crossings through intrinsically three-dimensional structures. In this Letter we present a series of EHs observed simultaneously at four Magnetospheric Multiscale (MMS) spacecraft in the plasma sheet boundary layer. The simultaneous multispacecraft probing allows analysis, for the first time, of the 3-D configuration of EHs.

2. Observations

We consider MMS measurements on 27 September 2016 around 01:19:00 UT. The spacecraft were located in the plasma sheet boundary layer at $\mathbf{r}_{\mathrm{GSM}} \sim (-2.6, 9.8, 0.6)\ R_E$ on field lines mapping to the southern auroral zone. The separation between the spacecraft was a few kilometers during the considered time interval. We use measurements of the direct current-coupled magnetic field (128 samples per second) provided by Digital and Analogue Fluxgate Magnetometers (Russell et al., 2016), alternating current-coupled electric field (8,192 samples per second) provided by Axial Double Probe (Ergun et al., 2016), and Spin-Plane Double Probe (Lindqvist et al., 2016), electron and ion moments provided by the Fast Plasma Instrument (Pollock et al., 2016). The electric fields are presented in the field-aligned coordinate system (x, y, and z) with the z axis along the local magnetic field, the x axis in the plane of a dipole magnetic field line, and the y axis generally in the westward direction.

Figure 1 provides a global context for the intense electric field fluctuations that we analyze in detail. Figure 1a presents the quasi-static magnetic field **B** in the geocentric solar magnetospheric (GSM) coordinate system measured aboard MMS#4 for a few minutes around 01:19:00 UT and the magnetic field B_L in the lobes computed using the vertical pressure balance, $B_L^2 = B^2 + 8\pi n_e(T_e + T_p)$, where n_e is the electron density and T_e and T_p are electron and ion temperatures (not shown). We use four-spacecraft measurements to compute the current density by the curlometer technique (e.g., Chanteur, 2000) and determine current densities parallel and perpendicular to the magnetic field. Figures 1a and 1b show that the spacecraft were in the plasma

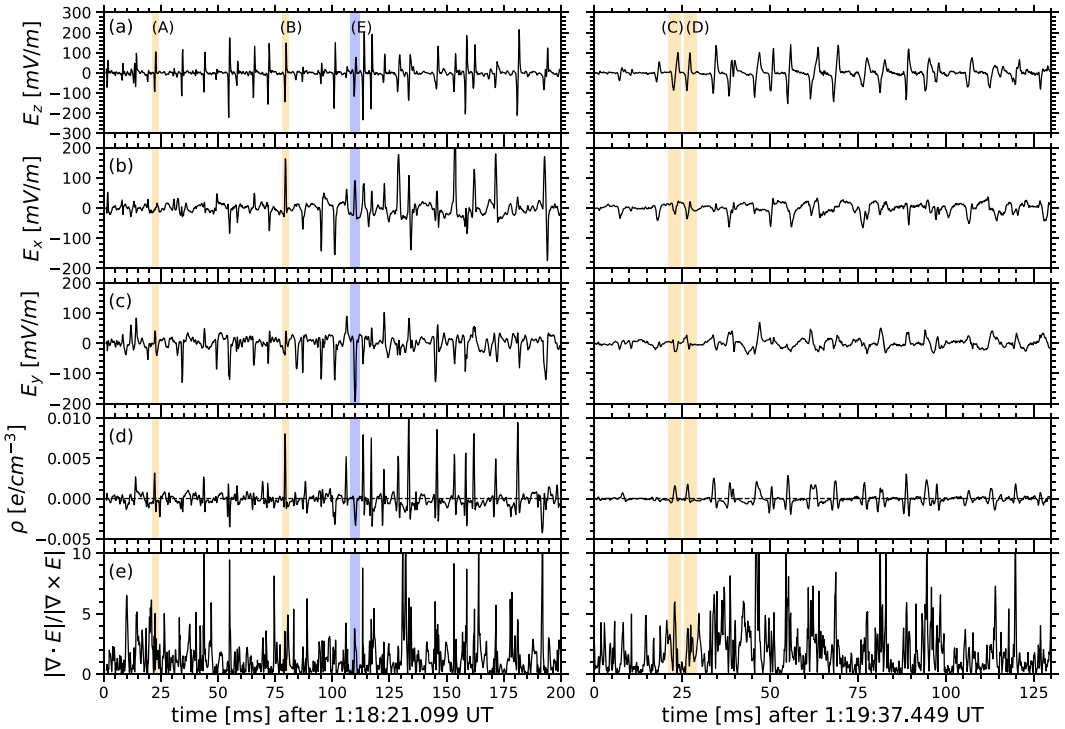

Figure 2. The expanded view of a few hundred millisecond intervals highlighted in Figure 1: (a) parallel and (b, c) perpendicular electric fields measured aboard MMS#4; (d) the charge density estimate $\rho = \nabla \cdot \mathbf{E}/4\pi$ computed using electric fields measured at four MMS spacecraft; and (e) parameter $|\nabla \cdot \mathbf{E}|/|\nabla \times \mathbf{E}|$ indicating a general consistency with the electrostatic nature of the solitary waves. The highlighted solitary waves (A)–(D) are presented in Figure 4. MMS = Magnetospheric Multiscale.

sheet boundary layer ($B \sim B_L$) and became closer to the neutral sheet after 01:19:20 and 01:19:50 UT as $|B_x|$ decreased. The decreases of $|B_x|$ were associated with up to 300-nA/m^2 parallel currents, indicating (along with reversed plasma flows that are not shown) temporal variations of the magnetic field configuration in the plasma sheet. Figure 1c presents electric field fluctuations with amplitudes up to 200 mV/m observed around the intense parallel current regions, although there was no strict correlation between the current density and electric field intensity. Series of ESWs were observed during the three highlighted intervals. The rather noisy low-frequency electric field complicates analysis of ESW for the middle interval, and therefore, we focus on the two other highlighted intervals characterized by the following background plasma parameters: $n_e \lesssim 0.1$ cm^{-3}, $T_e \sim 1$ keV, and $\omega_p/\omega_c \sim 1$–2.

Figure 2 covers a few hundred milliseconds around the two highlighted time intervals. Figures 2a–2c present the electric fields measured aboard MMS#4 in the field-aligned coordinate system and show that the electric field fluctuations are produced by solitary waves with bipolar parallel and mostly unipolar perpendicular electric fields. The solitary waves are associated with ~10-pT magnetic field fluctuations (not shown), which is why they are ESW ($\delta E \gg c\delta B$). The perpendicular magnetic field fluctuations appear due to the Lorentz transformation (Andersson et al., 2009) and provide the ESW velocity estimates of a few thousand kilometers per second. Remarkably, the ESW are observed simultaneously at four MMS spacecraft (shown below). We use multispacecraft interferometry, that is, analysis of time lags between observations of the same ESW at different spacecraft, to estimate the ESW velocity and direction of propagation. The ESWs propagate with velocities 3,000–10,000 km/s antiparallel to **B** within about 10° (see the supporting information [SI] for details). It would be difficult to estimate the ESW velocities using the interferometry between voltage-sensitive probes separated by about 120-m antennas because the ESWs propagate too fast for the time lags between the probes to be determined reliably.

The electron phase space density measured during the ESW observation (see the SI) shows that there is a plateau in the phase space density of electrons with ~180° pitch angles in the energy range 100–1,000 eV (that is 6,000–20,000 km/s in terms of electron velocities). The fact that these energies correspond to the

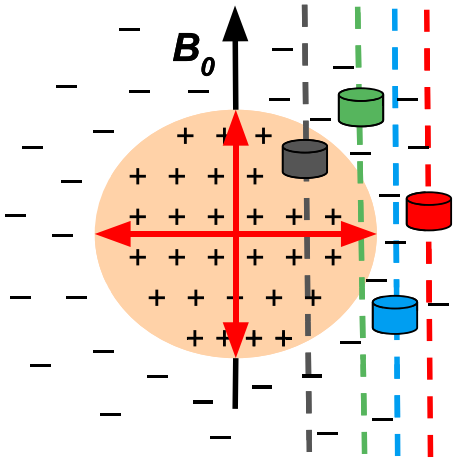

Figure 3. The schematic of an electron phase space hole (EH; red arrows indicate electric fields) and spacecraft crossings (dashed lines) due to quasi-parallel propagation of the EH with respect to the magnetic field. EHs are structures with a positive electrostatic potential localized in directions parallel and perpendicular to a local magnetic field. The plus/minus signs indicate the charge density: the EH is effectively a positively charged cloud screened by a negatively charged cloud.

ESW propagation velocities indicates that the ESWs are likely produced in a nonlinear stage of an instability driven by a few hundred electron-volt electrons streaming antiparallel to **B**. The instability belongs to the bump-on-tail type (e.g., Omura et al., 1996), rather than the Buneman-type, because the latter can only produce slow solitary waves propagating at $(m_e/m_i)^{1/3}j_{||}/en_e$ (e.g., Drake et al., 2003), which is less than ~1,500 km/s because, in our event, $j_{||} \lesssim 300$ nA/m^2. Because the ESWs propagate antiparallel to **B** and the parallel electric field of each ESW is first negative and then positive according to Figure 2a, the ESWs have positive electrostatic potentials. This indicates that the ESW are EHs. Schematics of EH is presented in Figure 3.

Simultaneous probing of EH at four MMS spacecraft allows estimating electric field gradients ∇E_x, ∇E_y, and ∇E_z by assuming that they are uniform over the MMS tetrahedron (the method is similar to the curlometer technique; see, e.g., Chanteur, 2000). The combinations of the gradients are used to compute $\nabla \cdot \mathbf{E}$ and $\nabla \times \mathbf{E}$. The charge density estimate $\rho = \nabla \cdot \mathbf{E}/4\pi$ presented in Figure 2d shows that the EHs are associated with either tripolar (− + −) charge densities expected for one-dimensional EHs or purely negative charge densities (see, e.g., EHs A–E). These charge densities correspond to different crossings of the four MMS spacecraft through the intrinsically three-dimensional EHs. The tripolar/negative charge densities correspond to crossings near/far from the EH center (Figure 3). Figure 2e shows that $|\nabla \cdot \mathbf{E}|/|\nabla \times \mathbf{E}|$ ~3–5 within EHs that is generally consistent with the electrostatic nature of these structures. The analysis by Robert et al. (1998) of the accuracy of the curlometer technique suggests that $|\nabla \cdot \mathbf{E}|/|\nabla \times \mathbf{E}|$ correlates with the accuracy of $\nabla \cdot \mathbf{E}$ estimate only statistically. Therefore, the accuracy of the charge density estimates is difficult to evaluate, but we stress that these estimates are consistent with those derived from the model used to fit the observed electric fields (shown below).

Figure 4 presents expanded views of EHs (A)–(D) and demonstrates that EHs are observed simultaneously at four MMS spacecraft. The velocities computed using the multispacecraft interferometry are indicated in the panels. The typical parallel scale of EH is computed as $d_{||} = v_h \cdot \Delta t/2$, where v_h is the EH velocity and Δt is the time lag between observing minimum and maximum of E_z (Δt is averaged over the four spacecraft). The parallel scales of EHs are indicated in the panels. Because the Debye length and electron thermal gyroradius are both about 1 km, the parallel scales of EHs are just a few Debye lengths or a few electron thermal gyroradii. The typical electric field amplitudes are about 100 mV/m, so the amplitudes of the maximum electrostatic potential along the spacecraft crossings are a few hundred volts.

3. Three-Dimensional Electron Hole Configuration

The theory does not pose significant restrictions on the 3-D distribution of the electrostatic potential of EHs (e.g., Chen et al., 2005). In single-spacecraft studies, EHs are often assumed axially symmetric with respect to a local magnetic field (e.g., Chen et al., 2005; Vasko et al., 2017). Statistical arguments have been invoked to estimate perpendicular scales of EHs based on numerous single-spacecraft crossings (Franz et al., 2000). The multispacecraft probing allows analyzing the 3-D configuration of EHs.

The axial symmetry of EHs (A)–(D) is tested by fitting the observed electric fields to a model distribution of the electrostatic potential:

$$\Phi(\mathbf{r},t) = \Phi_0 \exp\left[-(z - v_h t)^2/2d_{||}^2\right] \cdot \mathcal{H}(\mathcal{R}), \quad \mathcal{R}^2 = x'^2/d_{\min}^2 + y'^2/d_{\max}^2, \tag{1}$$

$$x' = (x - x_0)\cos\psi + (y - y_0)\sin\psi, \quad y' = -(x - x_0)\sin\psi + (y - y_0)\cos\psi$$

where v_h and $d_{||}$ have been evaluated, Φ_0 is the peak amplitude of the electrostatic potential, x_0 and y_0 determine the position of the EH center, angle ψ determines the orientation of minor and major axes of the elliptic cross section with respect to the field-aligned coordinates, and $d_{\min}$ and $d_{\max}$ are perpendicular scales corresponding to the minor and major axes. We have tried to fit the observed electric fields to various models and

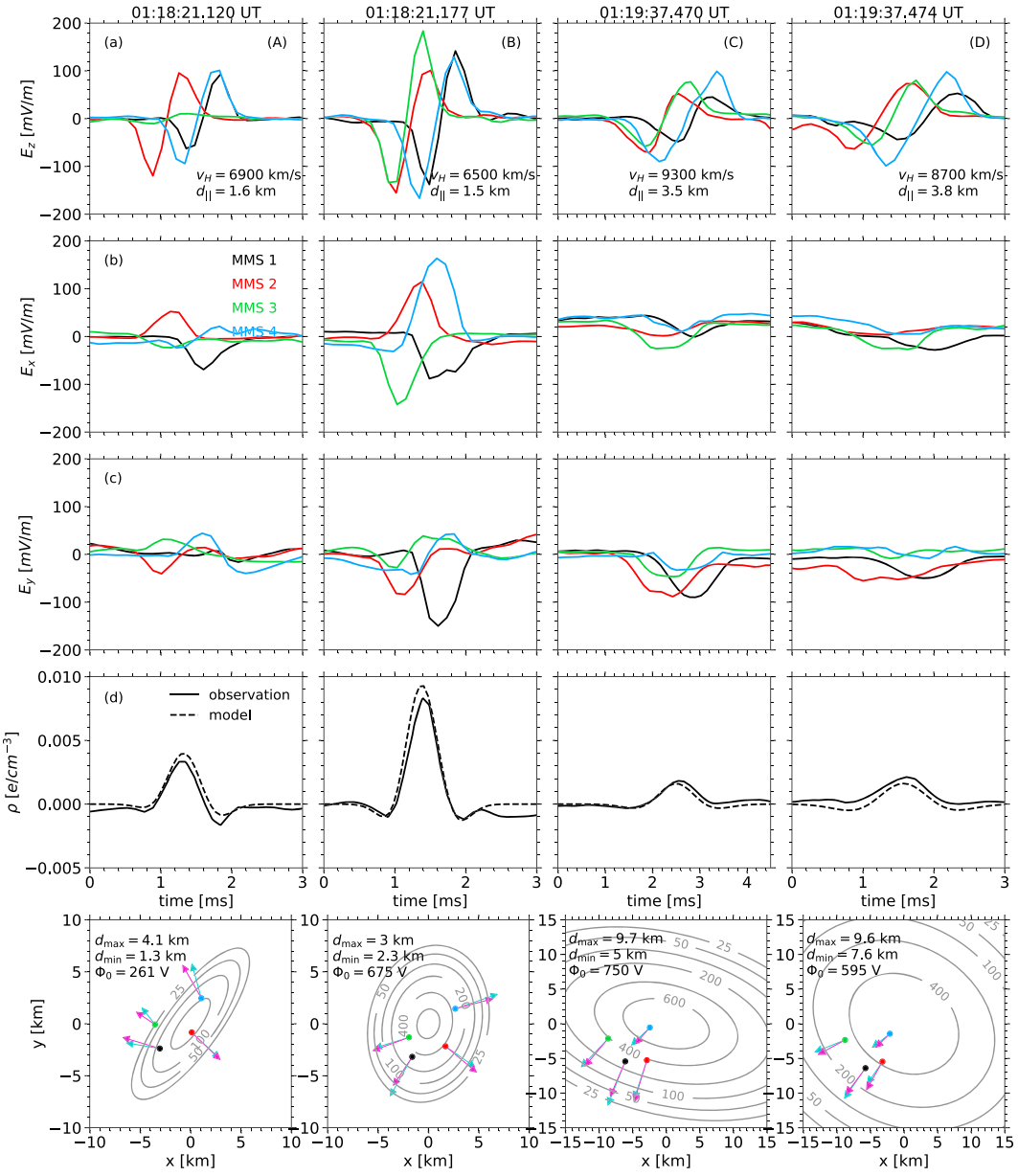

Figure 4. The simultaneous measurements of electron phase space holes (A)–(D) at four MMS spacecraft: (a)–(c) the electric field in the field-aligned coordinate system and (d) the charge density computed using the electric field measurements at four spacecraft (solid) and the charge density computed using the electric fields at four spacecraft according to the best fit model distribution (equation (1); dashed). The bottom panels present observed and best fit model electric fields (cyan and magenta arrows) in the plane perpendicular to the magnetic field, where $E_z = 0$. The equipotential contours (in unit of volts) of the best fit model are shown, and the best fit parameters d_{min}, d_{max} and Φ_0 are indicated. The field-aligned coordinate system is used in the bottom panels. MMS = Magnetospheric Multiscale.

found the best fit to be provided by the Gaussian model, $\mathcal{H} = \exp(-\mathcal{R}^2/2)$. Originally, we have used the axially symmetric model with four parameters (Φ_0, x_0, y_0 and $d_{min} = d_{max}$) and found that the fitting procedure converges to a global minimum. Then we have used the nonaxially symmetric model with six free parameters and searched for the best fit parameters around this global minimum (see the SI for details).

The bottom panels of Figure 4 present the observed and best fit model electric fields in the plane perpendicular to the magnetic field, where $E_z = 0$. The spacecraft positions and electric fields are in the field-aligned coordinate system with the origin in the EH center (x_0 and y_0). Also shown are the best fit parameters and equipotential curves of the model electrostatic potential. The electric field of EHs (B) and (D) is satisfactorily

fitted to almost axially symmetric models with d_{min} and d_{max} different by a factor of less than 1.3. On the other hand, EHs (A) and (C) are clearly non axially symmetric, because d_{min} and d_{max} differ by a factor of 2 to 3. The perpendicular scales are larger than the parallel scales by a factor of 2 to 3 in agreement with the gyrokinetic scaling relation $d_\perp/d_\parallel \sim (1+\omega_p^2/\omega_c^2)^{1/2}$, where $\omega_p \sim 1-2\,\omega_c$. The amplitudes of the electrostatic potentials are 250–750 V, which is quite comparable to ~1-keV electron temperature.

Figure 4d presents the charge densities computed using the technique similar to the curlometer technique (see the previous section) using the electric fields observed at four spacecraft and those given by the best fit models. These charge densities are in satisfactory agreement. The best fit models also reproduce the observed electric fields (see SI). On the time scales of the fast EHs, ions are essentially immobile, so the estimated charge densities are due to electron density deficiencies. Figure 4d indicates that the electron density deficiencies may reach values of $\sim 10^{-2}$ cm^{-3}, which is about 10% of the background electron density.

We note that the analysis of the 3-D configuration of EHs requires simultaneous observations of the electric fields at four spacecraft with sufficiently high signal-to-noise ratio. EHs (A)–(D) are good examples satisfying this criterion. We could not fit the electric fields of EH (E) to the 3-D model, because the electric fields observed at two of the spacecraft were too small (these spacecraft probed the EH rather far from the EH center). We have also failed to model many other EHs from the two selected intervals. Quite often, the EH velocities had large uncertainties that may have been due to either EH evolution during propagation from one spacecraft to another and/or complicated 3-D configurations different from the simple model (1).

4. Discussion and Conclusions

We have presented observations of EHs observed simultaneously at four MMS spacecraft in a region with intense parallel currents and fast plasma flows in the plasma sheet boundary layer. Similar EHs associated with intense parallel currents in the plasma sheet boundary layer have been recently reported by Le Contel et al. (2017), but the spacecraft separation of about 50 km did not allow simultaneous observations of the EHs at four MMS spacecraft. We have used multispacecraft interferometry to estimate the EH velocities and direction of propagation. Previous multispacecraft interferometry analyses have been restricted to two spacecraft and required assumptions on the direction of EH propagation (Norgren et al., 2015; Pickett et al., 2008). Using the multispacecraft interferometry we have found that the EHs propagate quasi-parallel to the magnetic field with velocities of a few thousands of kilometers per second and have parallel spatial scales of a few Debye lengths.

Multispacecraft probing has allowed analysis, for the first time, of the 3-D configuration of the EHs. We have estimated the charge densities associated with the EHs to find that they are consistent with the three-dimensional EH configuration: EH is effectively a positively charged cloud screened by a negatively charged cloud. For several of the EHs we have demonstrated that their 3-D configuration is adequately described by Gaussian distributions with elliptic cross section and two perpendicular scales that can differ by as much as a factor of 3. Thus, in contrast to the assumption often invoked in single-spacecraft studies (e.g., Chen et al., 2005; Le Contel et al., 2017; Vasko et al., 2017), the EHs are generally not axially symmetric. EHs exhibit $d_{max}/d_\parallel \sim 2-3$ and $d_{min}/d_\parallel \sim 1-2$ that is in satisfactory agreement with the gyrokinetic scaling relation (Franz et al., 2000) predicting $d_\perp/d_\parallel \sim 1.4-2.2$ for $\omega_p \sim 1-2\,\omega_c$.

In this letter we have presented detailed analysis of the 3-D configuration only for several EHs. In many other cases from the selected intervals, analyses have shown that EHs can evolve either in the course of propagation from one spacecraft to another and/or the 3-D configuration of the EHs is more complicated than that given by a simple Gaussian model. For these EHs we could not obtain a reliable estimate of velocity and could not infer the 3-D configuration. The approach presented in this letter will be valuable for analyses of properties of EHs observed in space plasmas.

Acknowledgments
The work was supported by NASA MMS Guest Investigator grant 80NSSC18K0155. We thank the MMS teams for the excellent data. The data are publicly available at https://lasp.colorado.edu/mms/public.

References

Andersson, L., Ergun, R. E., Tao, J., Roux, A., Lecontel, O., Angelopoulos, V., et al. (2009). New features of electron phase space holes observed by the THEMIS mission. *Physical Review Letters*, *102*(22), 225004. https://doi.org/10.1103/PhysRevLett.102.225004

Cattell, C., Dombeck, J., Wygant, J., Drake, J. F., Swisdak, M., Goldstein, M. L., et al. (2005). Cluster observations of electron holes in association with magnetotail reconnection and comparison to simulations. *Journal of Geophysical Research*, *110*, A01211. https://doi.org/10.1029/2004JA010519

Chanteur, G. (2000). Accuracy of fields gradient estimations by Cluster: Explanation of its dependency upon elongation and planarity of the tetrahedron. In R. A. Harris (Ed.), *Cluster-II workshop multiscale/multipoint plasma measurements, ESA special publication* (Vol. 449, pp. 265). France: CNRS.

Chen, L.-J., Pickett, J., Kintner, P., Franz, J., & Gurnett, D. (2005). On the width-amplitude inequality of electron phase space holes. *Journal of Geophysical Research*, *110*, A09211. https://doi.org/10.1029/2005JA011087

Drake, J. F., Swisdak, M., Cattell, C., Shay, M. A., Rogers, B. N., & Zeiler, A. (2003). Formation of electron holes and particle energization during magnetic reconnection. *Science*, *299*, 873–877. https://doi.org/10.1126/science.1080333

Ergun, R. E., Carlson, C. W., McFadden, J. P., Mozer, F. S., Muschietti, L., Roth, I., & Strangeway, R. J. (1998). Debye-scale plasma structures associated with magnetic-field-aligned electric fields. *Physical Review Letters*, *81*, 826–829. https://doi.org/10.1103/PhysRevLett.81.826

Ergun, R. E., Goodrich, K. A., Stawarz, J. E., Andersson, L., & Angelopoulos, V. (2015). Large-amplitude electric fields associated with bursty bulk flow braking in the Earth's plasma sheet. *Journal of Geophysical Research: Space Physics*, *120*, 1832–1844. https://doi.org/10.1002/2014JA020165

Ergun, R. E., Tucker, S., Westfall, J., Goodrich, K. A., Malaspina, D. M., Summers, D., et al. (2016). The axial double probe and fields signal processing for the MMS mission. *Space Science Reviews*, *199*, 167–188. https://doi.org/10.1007/s11214-014-0115-x

Fox, W., Porkolab, M., Egedal, J., Katz, N., & Le, A. (2008). Laboratory observation of electron phase-space holes during magnetic reconnection. *Physical Review Letters*, *101*(25), 255003. https://doi.org/10.1103/PhysRevLett.101.255003

Franz, J. R., Kintner, P. M., Seyler, C. E., Pickett, J. S., & Scudder, J. D. (2000). On the perpendicular scale of electron phase-space holes. *Geophysical Research Letters*, *27*, 169–172. https://doi.org/10.1029/1999GL010733

Graham, D. B., Khotyaintsev, Y. V., Vaivads, A., & Andr'e, M. (2016). Electrostatic solitary waves and electrostatic waves at the magnetopause. *Journal of Geophysical Research: Space Physics*, *121*, 3069–3092. https://doi.org/10.1002/2015JA021527

Le Contel, O., Nakamura, R., Breuillard, H., Argall, M. R., Graham, D. B., Fischer, D., et al. (2017). Lower hybrid drift waves and electromagnetic electron space-phase holes associated with dipolarization fronts and field-aligned currents observed by the Magnetospheric Multiscale mission during a substorm. *Journal of Geophysical Research: Space Physics*, *122*, 12. https://doi.org/10.1002/2017JA024550

Lindqvist, P.-A., Olsson, G., Torbert, R. B., King, B., Granoff, M., Rau, D., et al. (2016). The spin-plane double probe electric field instrument for MMS. *Space Science Reviews*, *199*, 137–165. https://doi.org/10.1007/s11214-014-0116-9

Malaspina, D. M., Ukhorskiy, A., Chu, X., & Wygant, J. (2018). A census of plasma waves and structures associated with an injection front in the inner magnetosphere. *Journal of Geophysical Research: Space Physics*, *123*, 2566–2587. https://doi.org/10.1002/2017JA025005

Malaspina, D. M., Wygant, J. R., Ergun, R. E., Reeves, G. D., Skoug, R. M., & Larsen, B. A. (2015). Electric field structures and waves at plasma boundaries in the inner magnetosphere. *Journal of Geophysical Research: Space Physics*, *120*, 4246–4263. https://doi.org/10.1002/2015JA021137

Matsumoto, H., Kojima, H., Miyatake, T., Omura, Y., Okada, M., Nagano, I., & Tsutsui, M. (1994). Electrotastic solitary waves (ESW) in the magnetotail: BEN wave forms observed by GEOTAIL. *Geophysical Research Letters*, *21*, 2915–2918. https://doi.org/10.1029/94GL01284

Mozer, F. S., Agapitov, O. V., Artemyev, A., Drake, J. F., Krasnoselskikh, V., Lejosne, S., & Vasko, I. (2015). Time domain structures: What and where they are, what they do, and how they are made. *Geophysical Research Letters*, *42*, 3627–3638. https://doi.org/10.1002/2015GL063946

Mozer, F. S., Ergun, R., Temerin, M., Cattell, C., Dombeck, J., & Wygant, J. (1997). New features of time domain electric-field structures in the auroral acceleration region. *Physical Review Letters*, *79*, 1281–1284. https://doi.org/10.1103/PhysRevLett.79.1281

Norgren, C., André, M., Vaivads, A., & Khotyaintsev, Y. V. (2015). Slow electron phase space holes: Magnetotail observations. *Geophysical Research Letters*, *42*, 1654–1661. https://doi.org/10.1002/2015GL063218

Omura, Y., Matsumoto, H., Miyake, T., & Kojima, H. (1996). Electron beam instabilities as generation mechanism of electrostatic solitary waves in the magnetotail. *Journal of Geophysical Research*, *101*, 2685–2698. https://doi.org/10.1029/95JA03145

Pickett, J., Chen, L., Kahler, S., Santolík, O., Gurnett, D., Tsurutani, B., & Balogh, A. (2004). Isolated electrostatic structures observed throughout the Cluster orbit: Relationship to magnetic field strength. *Annales Geophysicae*, *22*, 2515–2523. https://doi.org/10.5194/angeo-22-2515-2004

Pickett, J. S., Chen, L.-J., Mutel, R. L., Christopher, I. W., SantolíK, O., Lakhina, G. S., et al. (2008). Furthering our understanding of electrostatic solitary waves through cluster multispacecraft observations and theory. *Advances in Space Research*, *41*, 1666–1676. https://doi.org/10.1016/j.asr.2007.05.064

Pollock, C., Moore, T., Jacques, A., Burch, J., Gliese, U., Saito, Y., et al. (2016). Fast plasma investigation for magnetospheric multiscale. *Space Science Reviews*, *199*, 331–406. https://doi.org/10.1007/s11214-016-0245-4

Robert, P., Dunlop, M. W., Roux, A., & Chanteur, G. (1998). Accuracy of current density determination. *ISSI Scientific Reports Series*, *1*, 395–418.

Russell, C. T., Anderson, B. J., Baumjohann, W., Bromund, K. R., Dearborn, D., Fischer, D., et al. (2016). The magnetospheric multiscale magnetometers. *Space Science Reviewss*, *199*, 189–256. https://doi.org/10.1007/s11214-014-0057-3

Schamel, H. (1986). Electron holes, ion holes and double layers. Electrostatic phase space structures in theory and experiment. *Physics Reports*, *140*, 161–191. https://doi.org/10.1016/0370-1573(86)90043-8

Vasko, I. Y., Agapitov, O. V., Mozer, F. S., Artemyev, A. V., Drake, J. F., & Kuzichev, I. V. (2017). Electron holes in the outer radiation belt: Characteristics and their role in electron energization. *Journal of Geophysical Research: Space Physics*, *122*, 120–135. https://doi.org/10.1002/2016JA023083

Vasko, I. Y., Krasnoselskikh, V. V., Mozer, F. S., & Artemyev, A. V. (2018). Scattering by the broadband electrostatic turbulence in the space plasma. *Physics of Plasmas*, *25*(7), 072903. https://doi.org/10.1063/1.5039687